www.sciencetranslationalmedicine.org/cgi/content/full/3/112/112ra122/DC1

Supplementary Materials for

Age-Related Intimal Stiffening Enhances Endothelial Permeability and Leukocyte Transmigration

John Huynh, Nozomi Nishimura, Kuldeepsinh Rana, John M. Peloquin, Joseph P. Califano, Christine R. Montague, Michael R. King, Chris B. Schaffer, Cynthia A. Reinhart-King*

*To whom correspondence should be addressed. E-mail: cak57@cornell.edu

Published 7 December 2011, *Sci. Transl. Med.* **3**, 112ra122 (2011)
DOI: 10.1126/scitranslmed.3002761

The PDF file includes:

SUPPLEMENTARY METHODS

Measurement of endothelial permeability

Two-day post-confluent bovine aortic endothelial cells (BAECs) on polyacrylamide gels were immersed in 10 μM 40 kDa FITC-dextran (Sigma-Aldrich). Confocal z-slice images (512 x 512 pixels) were obtained on a Leica TCS SP2 system equipped with a 40× dipping lens. Using ImageJ (NIH, v. 1.42q) a 50×400 pixel rectangular box was drawn directly above the cell layer and the average pixel intensity, which represents the intensity of 10 μM FITC-dextran, was recorded. A second box of width 400 pixels was then drawn directly below the cell layer and encompassed the entire height of the polyacrylamide gel, which represented the average pixel intensity of FITC-dextran that had permeated through the cell monolayer into the gel. Dextran accumulation was calculated as the average pixel intensity within the gel divided by the average pixel intensity above the gel. Relative permeability values were then calculated as the dextran accumulation values of cell-seeded gels normalized to cell-free gels.

Histology and atomic force microscopy indentation of mouse thoracic aortas

Mouse thoracic aortas were de-endothelialized by gentle scraping using a cotton-tipped applicator. To verify de-endothelialization, scraped and unscraped samples were fixed in 3.7% buffered formaldehyde and submitted to the university's histology service for routine hematoxylin & eosin (H&E) staining. Images were acquired using an Olympus AX70 microscope with a 40× objective and an Optronics Microfire digital camera. Scraped samples purposed for indentation testing were bonded to a glass substrate using Loctite gel adhesive (Henkel Corporation) and kept submerged in PBS.

The stiffness of the subendothelium was measured by atomic force microscopy

indentation. A PicoPlus II scanning probe microscope (Agilent Technologies) and Au-coated SiN 0.12 N/µm cantilevers modified with 10-µm diameter polystyrene beads (Novascan) were used. Photodetector sensitivity was calibrated using force curves taken in PBS on a rigid substrate. The cantilever spring constant k_c (equation S1) was calibrated using Hutter's thermal noise method with corrections for cantilever tilt and optically-measured deflection (*S1-S3*).

$$k_c = 0.8174 \frac{k_B T}{\langle z^2 \rangle} \left(1 - \frac{3R}{2L} \tan\alpha\right)^{-1} \cos^2\alpha, \qquad \text{(eqn. S1)}$$

where k_B is Boltzmann's constant, T is temperature, $\langle z^2 \rangle$ is mean squared displacement of the primary bending mode, R is tip radius, L is cantilever length, and α is cantilever tilt angle. The calibrated spring constants were in the range of 0.10–0.11 N/m. Indentation speed was 1 µm/s. All testing was done at room temperature and within 12 hours of animal death. In this window, we believe mechanical properties were maintained, as previous data suggests that when arteries are tested within several hours of isolation at temperatures between 22 and 37°C, there are no detectable changes in their mechanical properties (*S4, S5*). Others have used similar transport procedures for testing of the medial layer and do not report any issue with cell viability (*S6, S7*). Additionally, other groups have used artery segments stored for longer times (>24 h) without loss of the smooth muscle cell contractile phenotype (*S8, S9*).

Indentation force curves were analyzed using the Hertz model, which is appropriate for a spherical indenter. The contact point was chosen visually and the point-by-point modulus E_{pp} calculated by fitting each data point individually to E_{pp} (equation S2):

$$E_{pp} = \frac{3F(1-\upsilon^2)}{4R^{1/2}\delta^{3/2}}, \qquad \text{(eqn. S2)}$$

where δ is indent depth and υ is Poisson's ratio. Incompressibility was assumed (υ = 0.5). The shape of the E_{pp} vs. δ plot is sensitive to errors in the contact point (*S10*). If an erroneous contact

point was indicated, the contact point was corrected. Curves in which the indenter failed to deform the tissue were discarded. A single indentation modulus value E was calculated for each indentation site by interpolating the E_{pp} vs. δ plot with a 5-point moving average, calculating an average $\underline{E_{pp}}$ vs. δ curve, and averaging E_{pp} over all δ. The resulting E is a measure of the indented site's overall stiffness.

Stiffness measurements of polyacrylamide gels

Steel balls (Abbott Ball Co.) with known density, ρ = 7,200 kg/m^3, and radius, R = 0.32 mm, were placed on polyacrylamide gels embedded with 0.5-µm fluorescent beads. A microscope was used to measure the indentation depth, δ, of the steel balls as they were magnetically removed from the gels as has previously been described (*S11, S12*). Gel stiffnesses were then calculated using the Hertz model for spherical contact. Recorded values of δ were inputted into the equation for Young's modulus, E (equation S3):

$$E = \frac{3F(1-\upsilon^2)}{4R^{1/2}\delta^{3/2}}, \qquad \text{(eqn. S3)}$$

where the Poisson's ratio, v, for polyacrylamide was assumed to be 0.3 (*S13*), and $F = \rho g(V - V_{cap})$, where g is 9.81 m/s^2, V is the volume of the steel ball, and V_{cap} is the indentation volume.

Flow chamber assembly and leukocyte rolling experiments

Human umbilical vein endothelial cells (HUVECs) on polyacrylamide gels were stimulated with 0.1 ng/ml recombinant human TNF-α (R&D Systems) for 6 h. A rectangular parallel-plate flow chamber (GylcoTech) with a gasket of size 0.254 cm × 1 cm × 6 cm (h × w × l) was carefully assembled over polyacrylamide gels and held together by vacuum. The flow chamber assembly

was secured onto the stage of an Olympus IX81 microscope equipped with a Hitachi CCD camera (KP-M1AN) connected to a DVD recorder (DVO-1000MD, Sony Electronics). A syringe pump (KDS 230, IITC Life Science) was used to control the flow rate of the cell suspension. Neutrophils at a concentration of 150,000 cells/ml flow buffer (0.5% human serum albumin (HSA, Sigma-Aldrich), 10 mM HEPES and 2 mM $CaCO_3$ in Hank's Balanced Salt Solution were perfused at a wall shear stress of 2 dyn/cm^2 for a total period of 7 min. "Rolling" cells were defined as those observed to translate in the direction of flow with an average velocity less than 50% of the calculated hydrodynamic free stream velocity. During flow, 79–96 random fields of view (640 × 480 pixels, 1.52 pixel/µm) were recorded using a 20× objective (NA 0.4, Olympus).

SUPPLEMENTARY FIGURES

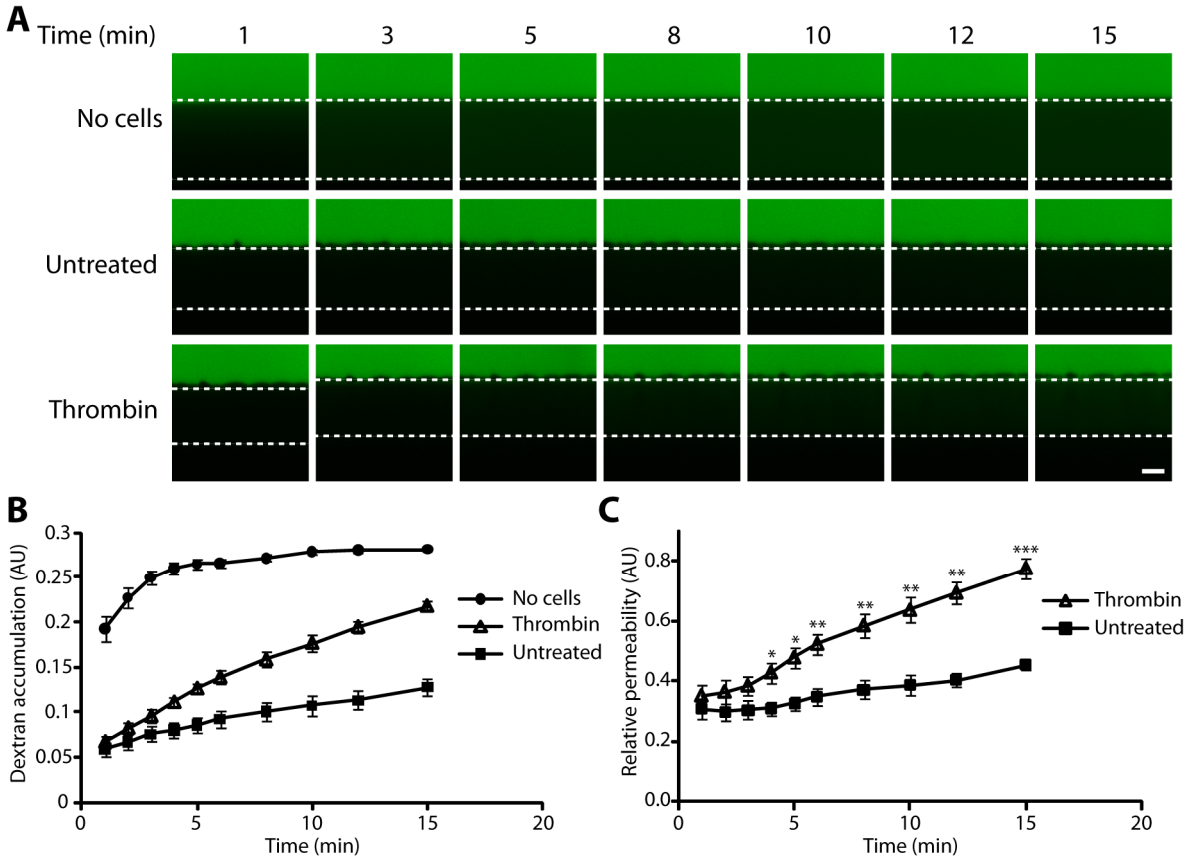

Fig. S1. Endothelial permeability measurements. **(A)** Representative time lapse z-sections of 5-kPa polyacrylamide gels with or without bovine aortic endothelial cell monolayers, as well as cells treated with thrombin (4 U/ml), immersed in FITC-dextran. Dashed lines represent top and bottom edges of the gel. Scale bar, 20 µm. **(B)** Quantification of FITC-dextran accumulation with respect to time in 5 kPa gels without cells (solid circles), with cells treated with thrombin (open triangles), and with untreated cells (solid squares). Data are means ± SEM. **(C)** Permeability values of thrombin-treated (open triangles) or untreated (solid squares) cells cultured on 5-kPa substrates normalized by the dextran accumulation values of the gels without cells. Data are means ± SEM. **P* < 0.05, ***P* < 0.01, ****P* < 0.001 (Student's *t* test) comparing thrombin-treated to untreated groups.

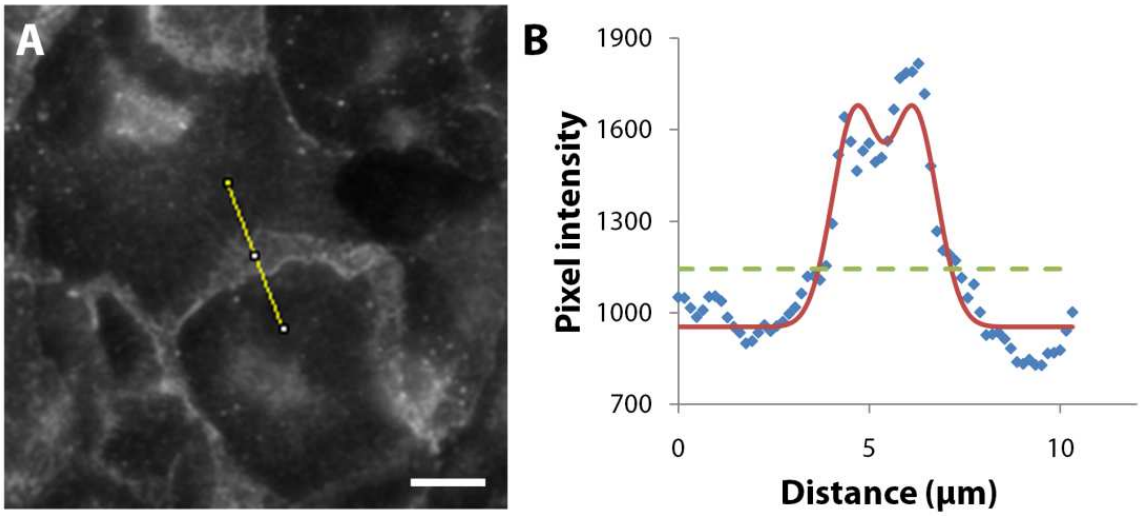

Fig. S2. VE-cadherin junctional gap width measurement. **(A)** VE-cadherin immunostaining of bovine aortic endothelial cells cultured on polyacrylamide gels. Scale bar, 5 µm. **(B)** Blue dots represent the pixel intensity profile of the yellow line drawn in (A), whereas the red line represents a two-Gaussian fit calculated using MATLAB. The junction width was considered as the width of the fitted curve at 20% above baseline intensity, as indicated by the dashed green line.

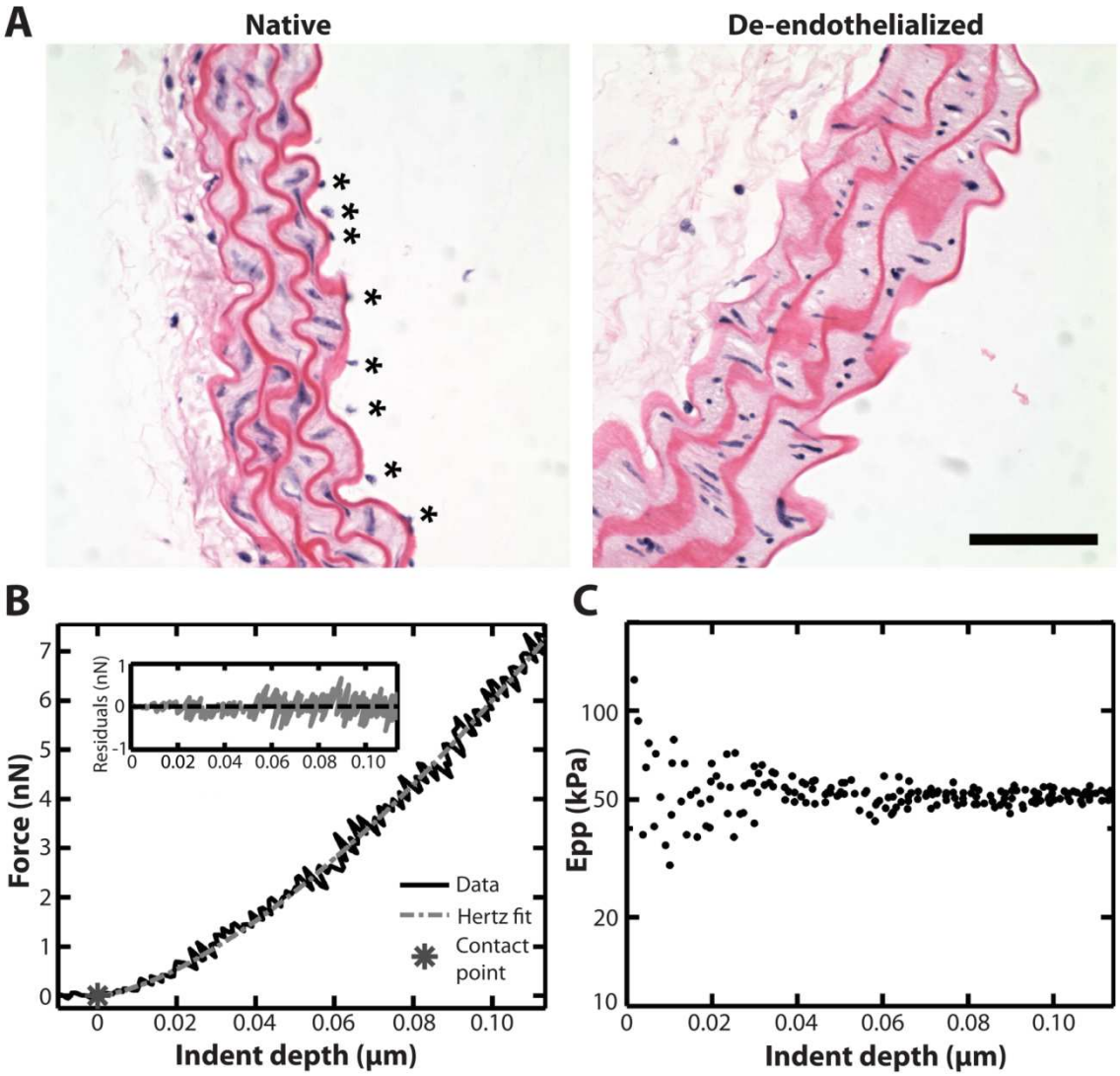

Fig. S3. Histology and AFM indentation of mouse thoracic aorta. **(A)** H&E staining of native and de-endothelialized aorta to show successful removal of ECs with minimal damage to underlying ECM. The section is perpendicular to the flow axis. Gentle scraping with a cotton applicator removes the ECs (asterisks) from the artery lumen, exposing the subendothelium for indentation. Scale bar, 50 μm. **(B)** Example least-squares fit of the Hertz model to AFM data, which shows the validity of the Hertz contact equation as a method to calculate the indentation modulus of mouse aortas. Insert: Residual error of the fit. **(C)** Example point-by-point modulus E_{pp} versus indentation depth plot obtained by individually fitting each data point in (B). After the initial noisy region ($\delta < 0.03$), the E_{pp} is approximately 50 kPa.

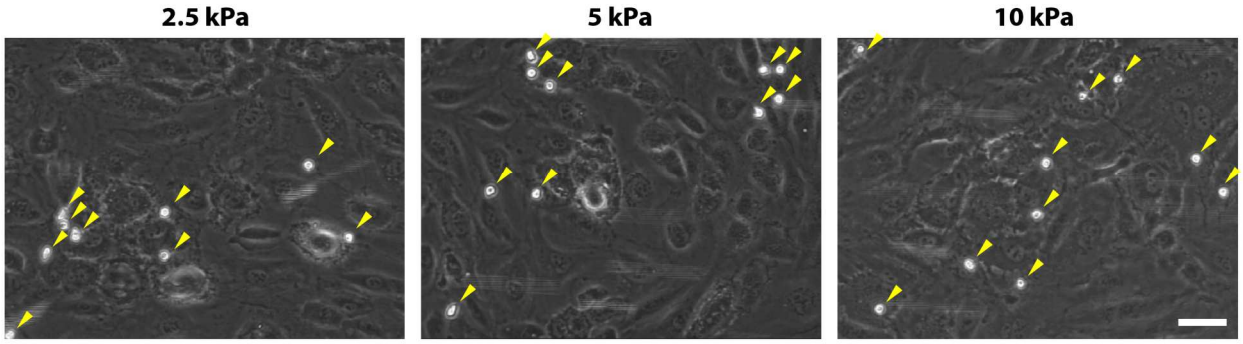

Fig S4. Leukocytes captured on HUVEC monolayers grown on polyacrylamide gels under flow. Representative micrographs of captured leukocytes. Yellow arrowheads indicate attached leukocytes. Leukocytes were rolled for 7 min in a parallel-plate flow chamber at 2 dyn/cm^2. Scale bar, 50 µm.

SUPPLEMENTAL REFERENCES

S1. J. L. Hutter, Comment on tilt of atomic force microscope cantilevers: effect on spring constant and adhesion measurements. *Langmuir* **21**, 2630-2632 (2005).

S2. J. L. Hutter, J. Bechhoefer, Calibration of Atomic-Force Microscope Tips. *Rev. Sci. Instrum.* **64**, 1868-1873 (1993).

S3. H. J. Butt, M. Jaschke, Calculation of Thermal Noise in Atomic-Force Microscopy. *Nanotechnology* **6**, 1-7 (1995).

S4. B. S. Gow, W. D. Castle, M. J. Legg, An improved microindentation technique to measure changes in properties of arterial intima during atherogenesis. *J. Biomech.* **16**, 451-458 (1983).

S5. J. A. Schaar, C. L. de Korte, F. Mastik, A. F. W. van der Steen, Effect of temperature increase and freezing on intravascular elastography. *Ultrasonics* **40**, 879-881 (2002).

S6. A. J. Engler, L. Richert, J. Y. Wong, C. Picart, D. E. Discher, Surface probe measurements of the elasticity of sectioned tissue, thin gels and polyelectrolyte multilayer films: correlations between substrate stiffness and cell adhesion. *Surface Sci.* **570**, 142-154 (2004).

S7. A. J. Engler, F. Rehfeldt, S. Sen, D. E. Discher, Microtissue elasticity: measurements by atomic force microscopy and its influence on cell differentiation. *Meth. Cell Biol.* **83**, 521-545 (2007).

S8. M. Basha, S. Chang, E. M. Smolock, R. S. Moreland, A. J. Wein, S. Chacko, Regional differences in myosin heavy chain isoform expression and maximal shortening velocity of the rat vaginal wall smooth muscle. *Am. J. Physiol. Regul. Integr. Comp. Physiol.* **291**, R1076-1084 (2006).

S9. E. M. Smolock, D. M. Trappanese, S. Chang, T. Wang, P. Titchnell, R. S. Moreland, siRNA-mediated knockdown of h-caldesmon in vascular smooth muscle. *Am. J. Physiol. Heart Circ. Physiol.* **297**, H1930-1939 (2009).

S10. S. L. Crick, F. C. Yin, Assessing micromechanical properties of cells with atomic force microscopy: importance of the contact point. *Biomech. Model Mechanobiol.* **6**, 199-210 (2007).

S11. C. A. Reinhart-King, M. Dembo, D. A. Hammer, Endothelial cell traction forces on RGD-derivatized polyacrylamide substrata. *Langmuir* **19**, 1573-1579 (2003).

S12. C. M. Lo, H. B. Wang, M. Dembo, Y. L. Wang, Cell movement is guided by the rigidity of the substrate. *Biophys. J.* **79**, 144-152 (2000).

S13. Y. Li, Z. B. Hu, C. F. Li, New Method for Measuring Poisson Ratio in Polymer Gels. *J. Appl. Polym. Sci.* **50**, 1107-1111 (1993).